

Effect of IDT position parameters on SAW yarn tension sensor sensitivity

Measurement and Control
2020, Vol. 53(9-10) 2055–2062
© The Author(s) 2020
Article reuse guidelines:
sagepub.com/journals-permissions
DOI: 10.1177/0020294020965620
journals.sagepub.com/home/mac



Bingbing Lei¹ , Wenke Lu², Zhibao Mian¹ and Wenxing Bao¹

Abstract

In this paper, the effect of the interdigital transducer (IDT) position parameters on the surface acoustic wave (SAW) yarn tension sensor sensitivity is investigated. The stress–strain characteristic of substrate was studied by the combination of finite element simulation and regression analysis method. According to this characteristic, the function relationship between the SAW yarn tension sensor sensitivity and the IDT position parameters was built using the regression analysis method. The monotonicity of the regression function was also given. On this basis, a novel sensitivity optimal scheme was proposed and solved by the quadratic programming method. Its solution demonstrates that the optimum sensitivity can be obtained when the IDT is 8.9 mm to the left side of the substrate and the IDT is 0.3 mm to the top edge of the substrate within a domain of the IDT position parameters. The SAW yarn tension sensor with corresponding IDT position parameters was fabricated to validate the correctness of the sensitivity optimal scheme. The measured results indicate that the SAW yarn tension sensor sensitivity can reach 813.69 Hz/g, which confirms that the novel scheme is effective.

Keywords

IDT position parameters, yarn tension sensor, regression function, sensitivity optimal, quadratic programming

Date received: 26 March 2020; accepted: 22 September 2020

Introduction

SAW sensors, which represent the merging of acoustic theory research, piezoelectric material achievements and electronic science and technology progress, display advantages such as high precision, simple structure, small size, easy integration, passivity, and good stability.^{1–4} Because SAW sensors are particularly sensitive to the environmental changes on the substrate surface, they are widely used in the detection of physical,⁵ chemical,⁶ and biological⁷ data. With the continuous increase in SAW sensor applications, the study of the aspects of theoretical enrichment,^{8,9} working mechanism innovation,¹⁰ simulation model improvement,¹¹ and working performance development¹² for SAW sensors has become a hot research topic.

Yarn tension is often the key factor in the process of yarn production.^{12–15} If too much force is supplied, the yarn will be snapped. If there is not enough force, the yarn will become loose and curled. This will result in lower quality of yarn and less production.^{16,17} Yarn tension is affected by so many elements that it is difficult to measure it. As a result, the accurate measurement of yarn tension is an urgent problem.¹⁸ The SAW yarn tension sensor was proposed¹⁹ for this purpose. It exhibits advantages such as low cost, reproducibility, and anti-interference, especially compared with traditional yarn tension sensors.

The yarn tension sensor sensitivity is of great significance to yarn production and quality.²⁰ As a result, the influence of the IDT position parameters on SAW yarn tension sensor sensitivity was investigated. After researching the substrate stress–strain characteristic, the regression function between sensor sensitivity and the IDT position parameters was established. Based on analyzing the function monotonicity, a novel scheme that can improve its sensitivity is proposed by optimizing the placement of the IDT on substrate.

Design

Figure 1 shows the design diagram of the SAW yarn tension sensor. A, B, C, Y, and S are the metal pedestal, the quartz spacer, the substrate, the yarn guide ring, and the sound absorbing adhesive, respectively. A mixture of epoxy resin and curing agent is used to glue

¹School of Computer Science and Engineering, North Minzu University, Yinchuan, China

²School of Information Science and Technology, Donghua University, Shanghai, China

Corresponding author:

Wenke Lu, School of Information Science and Technology, Donghua University, Shanghai 201620, China.
Email: luwenkelu@163.com



Creative Commons CC BY: This article is distributed under the terms of the Creative Commons Attribution 4.0 License (<https://creativecommons.org/licenses/by/4.0/>) which permits any use, reproduction and distribution of the work without

further permission provided the original work is attributed as specified on the SAGE and Open Access pages (<https://us.sagepub.com/en-us/nam/open-access-at-sage>).

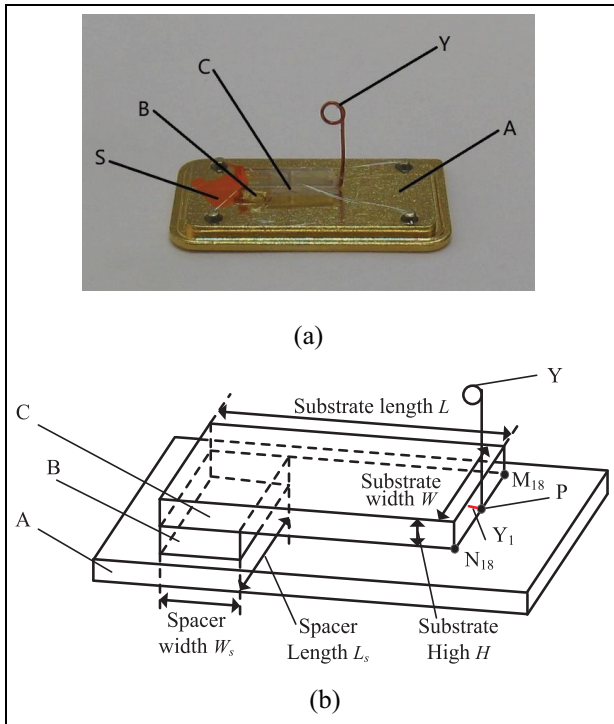


Figure 1. Sensor design diagram: (a) physical picture, (b) structural diagram.

them together. Y_1 is a part of the Y . Glue Y_1 to the bottom surface of the substrate C . The length of Y_1 is about 2 mm. Because its length is small and the finite element analysis results in this paper are mainly used for qualitative analysis, it is assumed that the force bearing point of the substrate is point P . Point P is located at the midpoint of line $M_{18}N_{18}$. The substrate length is $L = 17$ mm, width is $W = 5$ mm, and height is $H = 0.5$ mm. The spacer length is $L_s = 5$ mm, and width is $W_s = 5$ mm. The sensor is fabricated as a delay line oscillator. Its physical parameters are shown in Table 1.

When the yarn guide ring is applied to yarn tension F , it produces strain on the substrate. Substrate strain causes variations in the substrate mechanical and electrical properties. This changes the IDT intrinsic wavelength and SAW propagation speed on the substrate. Thus, the sensor output frequency f can be written as:

$$f = f_0 + \Delta f \quad (1)$$

where f_0 is the sensor center frequency, and Δf is output frequency shift.

As shown in Figure 2, the electrode-overlap envelope of the input IDT is weighted.^{12,14,16} Dummy electrodes are used. The output IDT is the uniform transducer. The length of the area occupied by the input and output IDTs is $L_I = 6.8$ mm, and the width is $W_I = 2.4$ mm. The area of the IDTs is D_I mm to the left side of the substrate, and D_I mm to the top edge of the substrate. The plane $M_0M_{17}N_{17}N_0$ is the upper surface of the substrate.

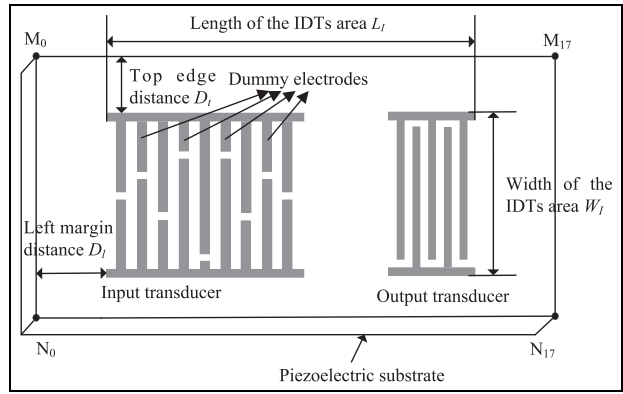


Figure 2. IDT design schematic diagram.

Table 1. Sensor physical parameters.

Parameter	Value
Substrate material	42° Y–X quartz
Metallization	3000 Å aluminum
Metallization ratio	0.5
Aperture	1.8 mm
Input IDT number	187.5
Output IDT number	160
IDT width	4.66 μm
Delay line length	0.3 mm
Center frequency	169.4 MHz

Table 2. Design parameters of sensors S1–S7.

Sensor	S1	S2	S3	S4	S5	S6	S7
D_l (mm)	1.4	3.9	6.4	3.9	3.9	1.4	8.9
D_t (mm)	0.3	0.3	0.3	1.3	2.3	2.3	2.3

There must be a sufficient number of data samples to build the function relationship between its sensitivity and the IDT position parameters. Too many data samples may also lead to overfitting. Meanwhile, the limitation of the sensor manufacturing conditions on the difference of IDT position parameters should be considered. So we use seven SAW yarn tension sensors, whose IDTs are placed at different positions on the substrate. The diameter of quartz wafer used in the factory is 2 inches (50.8 mm). To place eight sensor substrates or more during fabrication, the substrate size parameters cannot be much larger. Nor can the IDT position parameters. The IDT position parameters are also confined by the manufacture technology of cutting substrate. In addition, these parameters are usually selected at equal intervals. The proper design parameters of these sensors are shown in Table 2. Sensors S1–S6 are used to build the regression function and sensor S7 is used to validate the function.

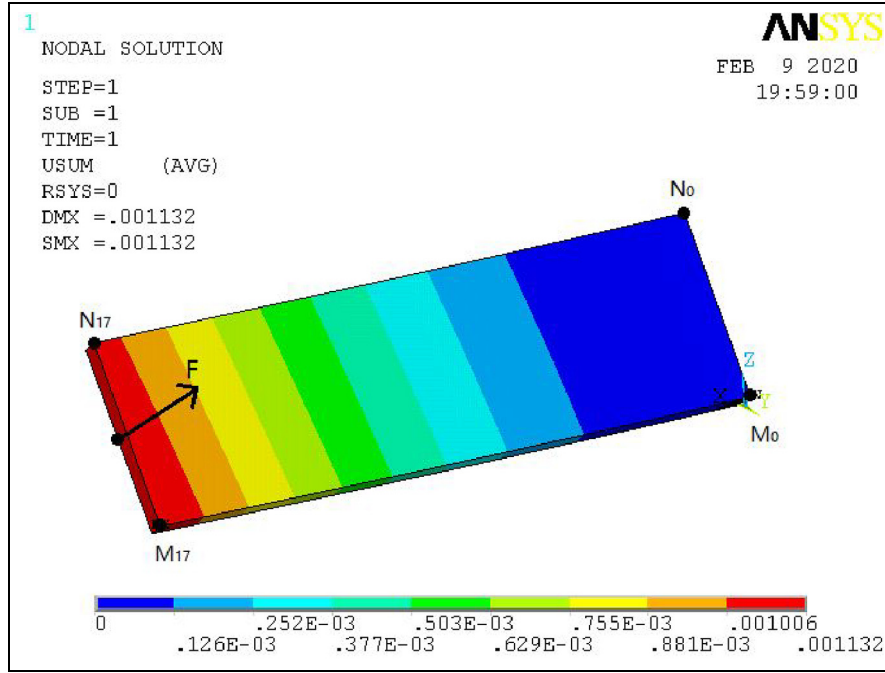


Figure 3. Stress–strain simulation result of substrate J1.

Effect of IDT position parameters on sensor sensitivity

Substrate stress–strain characteristic

The strain, induced by loading F , is so small that we assume the substrate is elongated along the SAW propagation direction. The elongation of the substrate is ΔL . The substrate strain can now be written as

$$\varepsilon = \frac{\Delta L}{L} \quad (2)$$

The substrate strain will cause the change of the sensor output frequency, so equation (1) can be expressed as²¹

$$f = f_0 + f_0 \varepsilon (k' - 1) \quad (3)$$

where k' is material coefficient, and it is a constant.

Compare equations (1) and (3), and it is found

$$\Delta f = f_0 \varepsilon (k' - 1) \quad (4)$$

The substrate strain will change linearly with yarn tension because piezoelectric crystal is elastomer. Thus, we have

$$\varepsilon = \varepsilon' F \quad (5)$$

where ε' is the substrate strain caused by unit tension, which is called substrate strain rate.

Substituting equation (5) into equation (4)

$$\Delta f = f_0 \varepsilon' (k' - 1) F \quad (6)$$

In equation (6), the term $f_0(k' - 1)\varepsilon'$ determines its frequency variation caused by unit load. The SAW yarn tension sensor sensitivity is then defined as

$$\sigma = f_0 \varepsilon' (k' - 1) \quad (7)$$

In equation (7), because f_0 and k' are constants, the value of the term ε' will determine the sensor sensitivity. Substitute equation (7) into equation (6)

$$\Delta f = \sigma F \quad (8)$$

Equation (8) needs to be solved by least square estimation. Thus, it is converted to

$$\Delta f = a + bF + e \quad (9)$$

where a , b are estimation coefficients, e is random error, and b should equal σ .

To analyze the stress–strain characteristic of substrate, the finite element model of the substrate stress–strain is simulated. The variable ε' can be gained from the ANSYS simulation result. The substrate, about 17 mm long, 5 mm wide and 0.5 mm high, is called J1. The ANSYS 13 was used to set up the stress–strain simulation model of J1 using element type SOLID185. The external load of the finite element model is defined as 1 g (unit tension $F = 1$), so the ANSYS simulation results are directly the substrate strain rate ε' according to equation (5). The metal film is not considered in the simulation model due to its thinness. The simulation result is shown in Figure 3.

We use line M_0M_{17} as an example, as shown in Figure 2. The M_0M_{17} line was divided by 17 1-mm segments. The 16 generated points are defined as points M_1 – M_{16} . M_0 was defined as the origin, and M_0M_{17} as

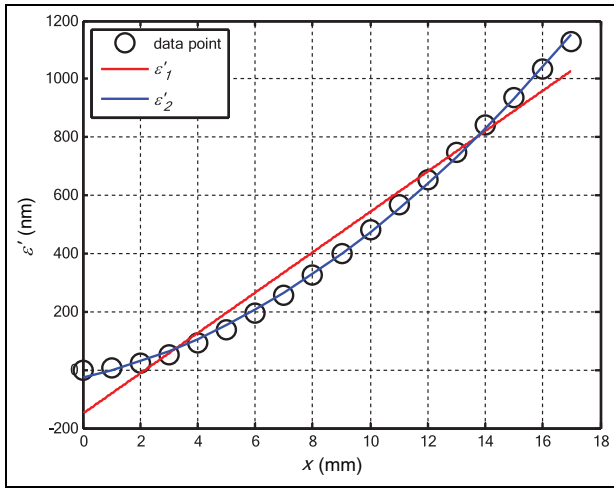


Figure 4. Curves between ε' and x .

the x -axis. Therefore the x coordinate at point M_0 is 0, the x coordinate at point M_1 is 1, and so on. The parameter x is defined as the x -axis coordinate. According to the simulation results shown in Figure 3, the substrate strain rate of those points can be obtained by clicking General Postproc \rightarrow List Results \rightarrow Nodal Solution in the ANSYS GUI.

The simulation output data reveals that as these points on line M_0M_{17} get further away from point M_0 , the magnitude of strain displacement induced by unit tension at these points increases. Therefore, the parameter x is independent variable, and ε' is dependent variable. Based on the causal relationship between the two, the substrate strain rate can be written as

$$\varepsilon' = k_0 + k_1x + k_2x^2 + \dots k_nx^n + e \quad (10)$$

where k_0, k_1, \dots, k_n are regression coefficients, and e is error.

Based on the simulation output data, the regression coefficients in equation (10) are solved by the least square method.

Let $n = 1$, we have

$$\varepsilon'_1 = -1472.32 + 442.58x \quad (11)$$

If $n = 2$, it is obtained

$$\varepsilon'_2 = -25.46 + 21.81x + 2.80x^2 \quad (12)$$

Figure 4 shows the fitting curves and the data points when $n = 1$ and $n = 2$.

In Figure 4, it is clear that the blue curve fits data points better than the red curve. Therefore equation (12) should be selected to reflect their functional relationship. Moreover, equation (12) is a quadratic function, which implies that the function relationship between them is nonlinear. This indicates that the distribution of the substrate strain is not uniform in the direction of the acoustic propagation path. In conclusion, according to equation (6), it is certain that this will cause the difference change of the IDT acoustic

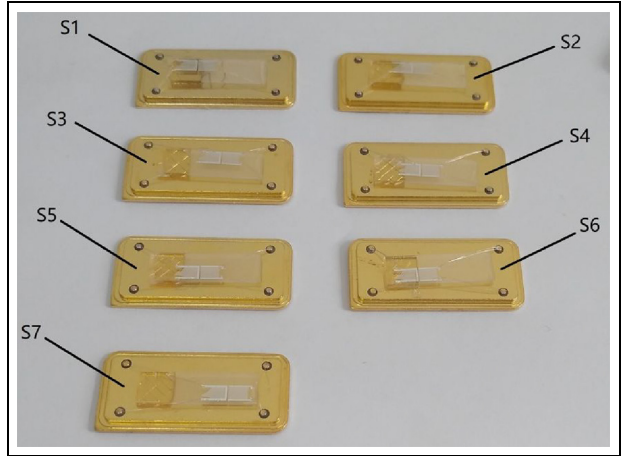


Figure 5. Fabricated physical form of sensors S1–S7.

synchronous frequency at a different x coordinate. Based on the above analysis, we conclude that the IDT position parameters will affect the SAW yarn tension sensor sensitivity.

Function between sensor sensitivity and IDT position parameters

As mentioned above, there should be a causal relationship between sensitivity and the IDT position parameters. This indicates that the parameter σ is explained variable, and the parameters D_l and D_t are explaining variables in the theory of multiple regression analysis. The multiple regression function between the two can be expressed as

$$\sigma = k_0 + k_1D_l + k_2D_t + k_3D_l^2 + k_4D_lD_t + k_5D_t^2 + e \quad (13)$$

where the k_0, k_1, \dots, k_5 are regression coefficients, and e is random error.

To build the model shown in equation (13), the data sample $((\sigma_i, D_{li}, D_{ti}), i = 1, \dots, n)$ should be given first. For this purpose, the output frequency shift of sensors S1–S7 is measured with yarn tension change using an Agilent E5061A network analyzer at 25°C. Their fabricated physical form is shown in Figure 5. The measured data are listed in Table 3.

To obtain equation (13), the sensitivity of sensors S1–S6 should be obtained first. According to Table 3, it is evident that the sensors with different placement of IDT show variations in output frequency change under the same yarn tension. This shows that the previous assumption is correct. It proves that there is a functional relationship between sensitivity σ and the IDT position parameters D_l and D_t .

Using S1 as an example, equation (9) is converted to

$$\Delta f_1 = a_1 + b_1F \quad (14)$$

Based on the data sample $((\Delta f_{1j}, F_j), j = 1, \dots, 11)$ of sensor S1 shown in Table 3, the parameters of

Table 3. Measurement data of sensors S1–S7.

F_j (g)		0	2	4	6	8	10	12	14	16	18	20
S1	Δf_{1j} (Hz)	0	1211	2502	3914	5241	6614	7919	9176	10,595	11,968	13,319
S2	Δf_{2j} (Hz)	0	1581	3095	4726	6113	7622	8997	10,464	11,914	13,317	14,686
S3	Δf_{3j} (Hz)	0	1658	3255	4951	6452	7919	9472	11,170	12,621	14,214	15,766
S4	Δf_{4j} (Hz)	0	1279	2710	4075	5557	6994	8264	9647	11,106	12,488	13,951
S5	Δf_{5j} (Hz)	0	1406	2846	4120	5604	6817	8073	9397	10,698	11,977	13,345
S6	Δf_{6j} (Hz)	0	1246	2514	3635	4872	5990	7056	8209	9412	10,592	11,759
S7	Δf_{7j} (Hz)	0	1393	2903	4532	6057	7570	8956	10,518	12,177	13,772	15,229

Table 4. Calculated results of sensors S1–S6.

Sensor	S1	S2	S3	S4	S5	S6
Sensitivity (Hz/g)	668.65	732.69	784.59	698.32	661.76	582.75
Determination coefficient	0.9998	0.9995	0.9998	0.9998	0.9996	0.9997
Relative error	2.9%	3.7%	2.8%	3.9%	3.8%	3.0%

equation (14) can be solved by least square method. The solutions are

$$\begin{aligned} a &= -99.36 \\ b &= 668.65 \end{aligned} \quad (15)$$

Substitute the solutions into equation (14)

$$\Delta f_1 = -99.36 + 668.65F \quad (16)$$

For Δf_1 , its determination coefficient is

$$R^2 = \frac{\sum_{j=1}^{11} (\Delta f_{1j}' - \overline{\Delta f_1})^2}{\sum_{j=1}^{11} (\Delta f_{1j} - \overline{\Delta f_1})^2} = 0.9998 \quad (17)$$

Equation (16) is the function between Δf_1 and F . The decision coefficient is so close to 1 that equation (16) is considered to fit well. As shown in equation (16), the sensitivity of the sensor S1 is 668.65 Hz/g. Its fitting curve is shown in Figure 6, and the relative error is 2.9%.

In the same way, the sensitivity of the others can be derived. Their fitting curves are also shown in Figure 6. The calculated results are listed in Table 4.

The determination coefficients shown in Table 4 are close to 1, indicating that the data are reliable. Thus, the experimental data sample $((\sigma_i, D_{li}, D_{ti}), i = 1, \dots, 6)$ is acquired as shown in Table 4. The software tool MATLAB is used to solve the least square estimation of the parameters in equation (13). The solutions are $k_0 = 640.87, k_1 = 29.86, k_2 = -44.29, k_3 = -0.97, k_4 = 2.99,$ and $k_5 = -1.09$. Those parameters are put in equation (13), which can be written as

$$\begin{aligned} \sigma &= 640.87 + 29.86D_l - 44.29D_t - 0.97D_l^2 \\ &\quad + 2.99D_lD_t - 1.09D_t^2 \end{aligned} \quad (18)$$

For parameter σ , its R^2 is

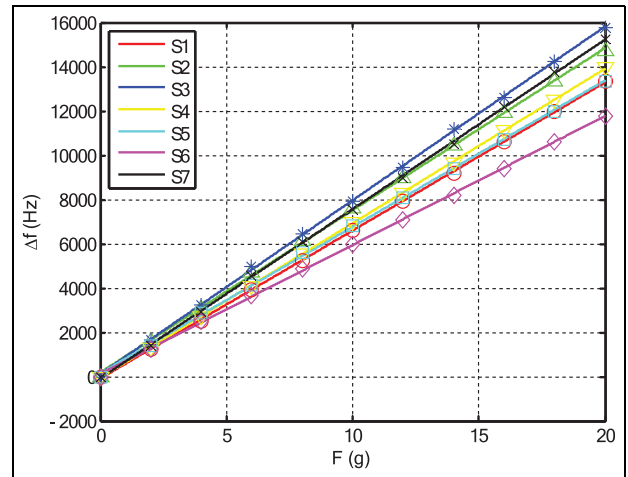


Figure 6. Fitting curves of sensors S1–S7.

$$R^2 = \frac{\sum_{i=1}^6 (\sigma_i' - \bar{\sigma})^2}{\sum_{i=1}^6 (\sigma_i - \bar{\sigma})^2} = 0.9998 \quad (19)$$

The R^2 is close to 1, which indicates that equation (18) can appropriately reflect the effect of the IDT position parameters on the sensor sensitivity. Its fitting surface is shown in Figure 7.

However, the limitation of the substrate actual size and manufacture technology to the IDT position parameters also needs to be considered. The domain of definition for equation (18) should be

$$\begin{aligned} 1.4 &\leq D_l \leq 8.9 \\ 0.3 &\leq D_t \leq 2.3 \end{aligned} \quad (20)$$

Sensor S7 is made to verify the functional relationship shown in equation (18). First, we obtain parameters $D_l = 1.4$ and $D_t = 2.3$ of S7 from Table 2. Then, it is calculated that the estimated value σ_7 is 783.36 Hz/g

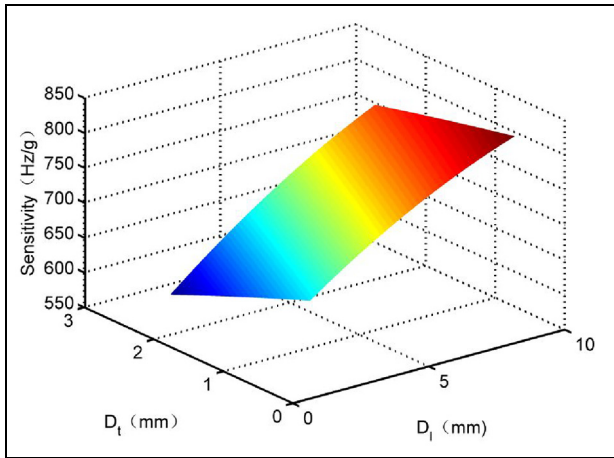


Figure 7. Curve between parameter σ and parameters D_l and D_t .

g according to equation (18). Finally, the data sample $((\Delta f_{7j}, F_j), j = 1, \dots, 11)$ of sensor S7 shown in Table 3 is used to solve equation (9). It is obtained as

$$\Delta f_7 = -97.27 + 765.25F \quad (21)$$

For Δf_7 , its determination coefficient is $R^2 = 0.9998$. Its fitting curve is shown in Figure 6. The actual sensitivity is 765.25 Hz/g. The relative error of sensor S7 is 2.9%. It can be seen that the estimated value is almost equal to the measured value. For sensor S7, the relative error between its actual sensitivity and estimated sensitivity is

$$\delta = \frac{783.36 - 765.25}{765.25} * 100\% = 2.4\% \quad (22)$$

The value δ is small, which demonstrates that the sensor sensitivity can be represented by the IDT position parameters. That is to say, the model shown in equation (18) can be used to express the functional relationship between parameter σ and parameters D_l and D_t within $\{(D_l, D_t) | 1.4 \leq D_l \leq 8.9, 0.3 \leq D_t \leq 2.3\}$.

It is found that equation (18) can be set up based on the IDT position parameters and the sensors sensitivity using the regression analysis method. For the other SAW force sensors, if we had related parameters, we could build the regression function too. Therefore, it can be concluded that the novel scheme can be applicable to SAW sensors with the different types of substrate material.

Effect of IDT position parameters on sensor sensitivity

For equation (18), the partial derivative σ'_l is given

$$\sigma'_l = \frac{\partial \sigma}{\partial D_l} = 29.86 - 1.94D_l + 2.99D_t \quad (23)$$

It is calculated that the parameter σ'_l is greater than zero because of $\{(D_l, D_t) | 1.4 \leq D_l \leq 8.9, 0.3 \leq D_t \leq 2.3\}$.

This illustrates that the parameter σ will monotonically increase with the parameter D_l . Consequently, we can make D_l larger to obtain higher sensitivity within the interval $\{(D_l, D_t) | 1.4 \leq D_l \leq 8.9, 0.3 \leq D_t \leq 2.3\}$.

Similarly, the partial derivative σ'_t is

$$\sigma'_t = \frac{\partial \sigma}{\partial D_t} = -44.29 + 2.99D_l - 2.18D_t \quad (24)$$

Since the value range of the parameters is $\{(D_l, D_t) | 1.4 \leq D_l \leq 8.9, 0.3 \leq D_t \leq 2.3\}$, we can calculate that $\sigma'_t < 0$. This shows the relationship between them is negative correlated. Then we put forward that the sensor sensitivity will increase with the parameter D_l decreasing.

Sensitivity optimization induced by IDT position parameters

Sensor sensitivity will vary with the change of the IDT position parameters. Therefore, sensitivity optimization was achieved by optimizing the IDT location parameters. The quadratic programming method was used to implement this scheme.

The function relationship between the dependent variable σ and the independent variables D_l and D_t is shown in equation (18). Parameter σ should be maximized, making it possible to gain optimization sensitivity. Hence, the objective function is given by

$$\max \sigma = 640.87 + 29.86D_l - 44.29D_t - 0.97D_l^2 + 2.99D_lD_t - 1.09D_t^2 \quad (25)$$

Due to the restrictions of substrate size and manufacturing technology, we choose equation (20) as the constraint condition.

The quadratic programming model shown in equations (25) and (20) is solved by Lingo software. The optimal solution is $\sigma = 824.35$, where $D_l = 8.9$ and $D_t = 0.3$. This means the maximum sensor sensitivity 824.35 Hz/g could be obtained when the IDT is 8.9 mm to left side of the substrate and the IDT is 0.3 mm to top edge of the substrate.

Sensor S8 was fabricated to verify the correctness of our scheme. Its design parameters are $L = 17$, $W = 5$, $H = 0.5$, $L_s = 5$, $W_s = 5$, $D_l = 8.9$, and $D_t = 0.3$. Its fabricated physical form is shown in Figure 8. In the same way, the fitting curve between Δf_8 and F is shown in Figure 9. Its sensitivity is given by

$$\Delta f_8 = 139.18 + 813.69F \quad (26)$$

The R^2 of Δf_8 is greater than 0.999, which proves that equation (26) fits the data well. Its measured sensitivity is 813.69 Hz/g, while the estimated value is 824.35 Hz/g. The difference is 10.66 Hz/g. Compared with the value 813.69 Hz/g, the difference is so small that the scheme can be considered effective. In addition, the sensitivity of sensor S8 is the largest of sensors S1-S8. Compared with the lowest sensitivity 582.75 Hz/g

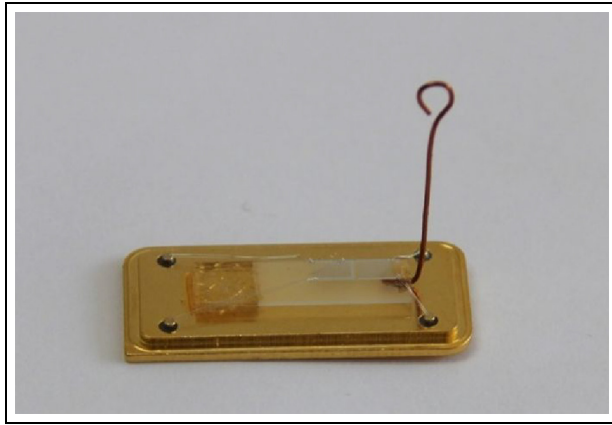


Figure 8. Fabricated physical form of sensor S8.

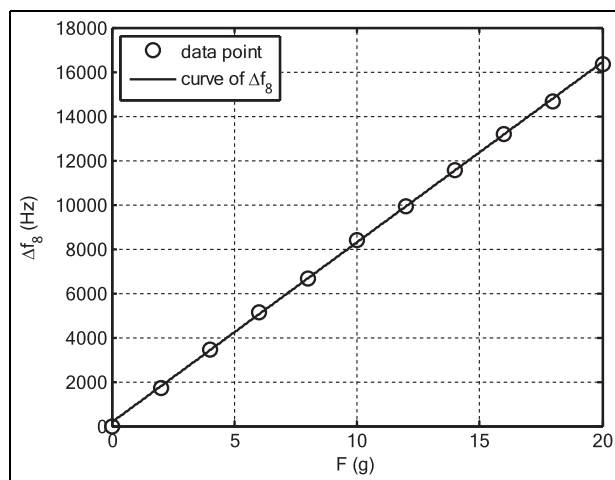


Figure 9. Curve between Δf_8 and F .

g (S6), this will improve sensitivity by 39%. This means that the scheme presented in this study can be used to improve sensor sensitivity by optimizing the IDT position parameters. In summary, the goal of obtaining greater sensitivity was achieved.

Conclusion

Through theoretical research and finite element simulation analysis, it is found that there is uneven distribution of the substrate strain rate in the direction of acoustic propagation path. Based on this conclusion, the regression function between SAW yarn tension sensor sensitivity and the IDT position parameters is established and validated. Using this model, the influence of the IDT position parameters on yarn tension sensor sensitivity was analyzed. The results suggest that if IDT is farther to the left side or closer to the top edge of the substrate, higher sensor sensitivity could be achieved. According to this regression function, the optimization of sensor sensitivity was achieved through a quadratic programming model. The results show that

the maximum sensitivity of 813.69 Hz/g was realized through optimizing the IDT position parameters. The modeling of substrate stress–strain characteristic is a subject worthy of further research.

Declaration of conflicting interests

The author(s) declared no potential conflicts of interest with respect to the research, authorship, and/or publication of this article.

Funding

The author(s) disclosed receipt of the following financial support for the research, authorship, and/or publication of this article: This article was supported by the Natural Science Foundation of Ningxia Province of China (Grant No. NZ1711, and No. 2020AAC02028), the National Natural Science Foundation of China (Grant No. 61461003), the Scientific Research Project of North Minzu University (Grant No. 2020XYZJK01), the Ningxia Key Discipline Projects of “Computer Application Technology” (Grant No. PY1607) and Major Projects of North Minzu University in 2018 (Grant No. 31519040263).

ORCID iD

Bingbing Lei  <https://orcid.org/0000-0002-2337-1619>

References

- Kondalkar VV, Li X, Park I, et al. Development of chipless, wireless current sensor system based on giant magnetoimpedance magnetic sensor and surface acoustic wave transponder. *Sci Rep* 2018; 8(1): 1–11.
- Benetti M, Cannata D, Verona E, et al. Highly selective surface acoustic wave e-nose implemented by laser direct writing. *Sens Actuators B Chem* 2019; 283: 154–162.
- Mathews SA, Bingham NS, Suess RJ, et al. Thermally induced magnetic anisotropy in Nickel films on surface acoustic wave devices. *IEEE Trans Magn* 2019; 55(2): 1–4.
- Li DJ, Tang YL, Ao DY, et al. Ultra-highly sensitive and selective H₂S gas sensor based on CuO with sub-ppb detection limit. *Int J Hydrogen Energy* 2019; 44(7): 3985–3992.
- Park KS. Nano- and submicro-sized three-dimensional shape measuring system using a saw-based capacitance sensor. *J Mech Sci Technol* 2018; 32(10): 4613–4619.
- Li DJ, Zu X, Ao D, et al. High humidity enhanced surface acoustic wave (SAW) H₂S sensors based on sol-gel CuO films. *Sens Actuators B Chem* 2019; 294: 55–61.
- Huang X, Farooq U, Chen J, et al. A surface acoustic wave pumped lensless microfluidic imaging system for flowing cell detection and counting. *IEEE Trans Biomed Circuits Syst* 2017; 11(6): 1478–1487.
- Zhgoon SA, Shvetsov AS and Sakharov SA. High-Temperature SAW resonator sensors: electrode design specifics. *IEEE Trans Ultrason Ferroelectr Freq Control* 2018; 65(4): 657–664.
- Chronopoulos D. Wave steering effects in anisotropic composite structures: direct calculation of the energy skew angle through a finite element scheme. *Ultrasonics* 2016; 73: 43–48.

10. Nguyen VH, Kaulen C, Simon U, et al. Single interdigital transducer approach for gravimetric SAW sensor applications in liquid environments. *Sensors* 2018; 17(12): 2931.
11. Toto S, Nicolay P, Morini GL, et al. Design and simulation of a wireless SAW-pirani sensor with extended range and sensitivity. *Sensors* 2019; 19(10): 2421.
12. Feng Y, Lu ZX, Lu W, et al. Study of the doubly clamped beam yarn tension sensor based on the surface acoustic wave. *IEEE Trans Ind Electron* 2018; 66(4): 3256–3264.
13. Wang Q, Li A, Li Y, et al. Microtension control for a yarn winding system with an IMC PID controller. *Mech Ind* 2019; 20(6): 609.
14. Lei BB, Lu WK, Zhu CC, et al. Optimization of sensitivity induced by substrate strain rate for surface acoustic wave yarn tension sensor. *IEEE Sens J* 2015; 15(9): 4769–4776.
15. Lu XZ, Lu WK and Zhu C. Compensated SAW yarn tension sensor. *IEEE Trans Instrum Meas* 2014; 63(12): 3162–3168.
16. Lei BB, Lu WK, Zhu CC, et al. A novel optimal sensitivity design scheme for yarn tension sensor using surface acoustic wave device. *Ultrasonics* 2014; 54(6): 1649–1655.
17. Wang Q, Lu CH, Huang R, et al. Computer vision for yarn microtension measurement. *Appl Opt* 2016; 55(9): 2393–2398.
18. Hossain M, Abdkader A, Nocke A, et al. N Measurement methods of dynamic yarn tension in a ring spinning process. *Fibres Text East Eur* 2016; 24(1): 36–43.
19. Lu WK, Lu XZ, Zhu CC, et al. Solving three key problems of the SAW yarn tension sensor. *IEEE Trans Electron Devices* 2012; 59(10): 2853–2855.
20. Liu X and Miao XH. Analysis of yarn tension based on yarn demand variation on a tricot knitting machine. *Text Res J* 2017; 87(4): 487–497.
21. Ye X, Fang L, Liang B, et al. Studies of a high-sensitive surface acoustic wave sensor for passive wireless blood pressure measurement. *Sens Actuators A Phys* 2011; 169(1): 74–82.